Design and Analysis of Electrical Braking Torque Limit Trajectory for Regenerative Braking in Electric Vehicles With PMSM Drive Systems

Kyoung-Min Choo and Chung-Yuen Won, *Senior Member, IEEE*

***Abstract*—In this article, an electrical braking torque limit trajectory is designed to improve the regenerative braking of electric vehicles based on a regenerative power analysis. Even though electric motors generally regenerate electric energy from kinetic energy, the drive system dissipates electric energy under certain low-speed operation conditions. This phenomenon has been addressed in many previous works and most of them compensate for this power dissipation region by modifying the electrical braking torque limit trajectory of the motor. However, the torque limit trajectory has never been considered based on a regenerative power analysis even though an inaccurate torque limit trajectory causes energy loss to the drive system. In this article, the regenerative power analysis for two major kinds of permanent magnet synchronous motor is performed. Afterward, torque limit trajectories are set based on this analysis so that batteries in electric vehicles can harvest the maximum regenerative energy in any circumstance. To verify the analysis and proposed torque limit trajectories, simulations and experiments are performed.**

***Index Terms*—Permanent magnet motors, synchronous motor drives, traction motor drives.**

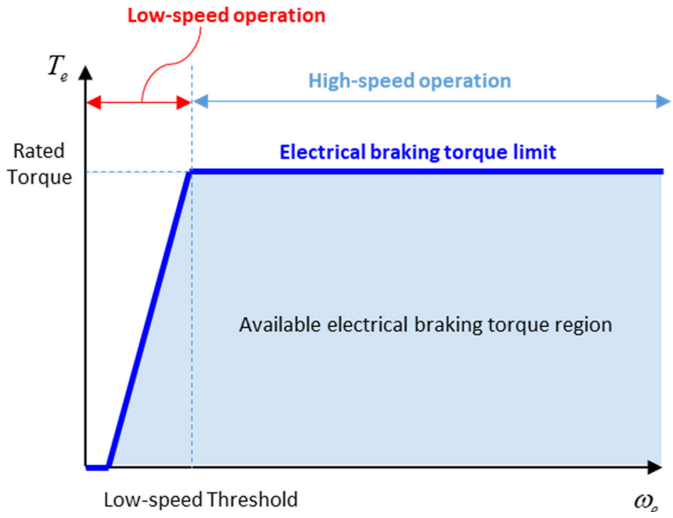

Fig. 1. General electrical braking torque limit trajectory for regenerative braking.

I. Introduction

REGENERATIVE braking gives one of the key advantages of electric vehicles; the drive system stores kinetic energy from the moving vehicle to the battery as electric energy for later use. This regenerative feature allows the total driving distance of electric vehicles to be extended. As the lack of power density in the battery is widely considered as the main reason for modern drivers' hesitation to choose electric vehicles over conventional internal combustion engine vehicles, extending driving distance without increasing battery capacity is an important issue. Regenerative braking for electric vehicles has been studied in many ways. In most of those studies, there is a common problem that the power of the battery is actually dissipated during the regenerative braking in a certain region of low-speed operation contrary to common sense. Since the regenerative energy during low-speed operation is small, this phenomenon is ignored in some of the studies. However, considering long driving times and frequent braking, which is more realistic, this power dissipation at low speed becomes a serious problem [1]. Also, since the advantages of regenerative braking is significant in heavy stop-and-go traffic [2], any improvement of low-speed regenerative energy can directly improve driving distance in such conditions. Generally, to solve the low-speed power dissipation problem, a torque limit is set, as shown in Fig. 1, where the limit value is constant in the high-speed region and decreases along with the motor speed in the low-speed region. Since low-speed regenerative energy is dependent on the region and slope of the limit torque, previous research focused on defining the low-speed power dissipation region so that it can be eliminated. In [1] and [3]–[5], the motor speed point where the battery current starts to get reversed is set as a low-speed boundary for the general torque limit shown in Fig. 1 and is defined as the low-speed cutoff point (LSCP) in [5]. As the name implies, regenerative braking stops the vehicle by removing electrical braking torque if the motor speed is lower than the LSCP. This method has become very popular because it gives a simple and practical

Manuscript received December 30, 2019; revised March 26, 2020; accepted May 7, 2020. Date of publication May 13, 2020; date of current version July 31, 2020. This work was supported by the National Research Foundation of Korea(NRF) grant funded by the Korea Government (MSIP) (No. 2019R1A2C2007216). Recommended for publication by Associate Editor J. Ye. *(Corresponding author: Chung-Yuen Won.)*

The authors are with the Department of Electronic and Electrical Engineering, School of Information and Communication Engineering, Sungkyunkwan University, Suwon 440-746, South Korea (e-mail: chuchoo@skku.edu; woncy@.skku.edu).

Color versions of one or more of the figures in this article are available online at https://ieeexplore.ieee.org.

Digital Object Identifier 10.1109/TPEL.2020.2994615

guideline to set the torque limit trajectory. In [6]–[10], the fact that LSCP moves under certain conditions was discovered, and regenerative braking methods with dynamic LSCP to maximize regenerative energy were proposed. However, those previous torque limiters based on LSCP could never achieve maximum regenerative power as the analysis in Section II shows. Since most low-speed power dissipation phenomenon, including LSCP, can be explained by analysis based on models of electric motors, it is also reasonable to set the torque limit trajectory using them. In previous analysis, the low back electromotive force (EMF) produced at low speed by the electric motor [11] and the state-of-charge of the battery are blamed for the low-speed power dissipation phenomenon [1]. Although the low power conversion efficiency of the inverter from small back EMF and battery copper loss may contribute to the slight decrements of the regenerative power in low-speed region, they are not sufficient to explain the power dissipation phenomenon. The author of [1] implies that the power dissipation region would differ according to the electric motor specification, which is true, but there was no specific analysis. In [12], the difference of LSCP is analyzed based on the environment the vehicle is in, such as wind speed and road slope angle. However, the analysis is too complicated to use just for compensation of LSCP, and LSCP is not dependent on the environment. In [9], LSCP is set based on an electric motor performance table to find the exact point for dynamic LSCP so that it can achieve the best performance from the electrical braking torque limit based on LSCP. In this electric motor performance table, maximum values for regenerative power appeared, but these maximum values were not used or mentioned in [9] since the purpose of the table was only to find LSCPs. Moreover, the proper analysis for LSCP was not performed because the table was made based on simulation results. In [13] and [14], regenerative power is analyzed for surface permanent magnet synchronous motor (SPMSM) and interior permanent magnet synchronous motor (IPMSM), respectively, which are two kinds of electric motors and widely used for the traction motors of electric vehicles because of their high power density and efficiency. According to the analysis in these papers, the type of electric motor, parameters of the motor, and electrical braking torque all have something to do with the maximum points of regenerative power, and, therefore, LSCP should be the same achieving less regenerative energy than the maximum point. Therefore, this article focuses not only on guidelines to design the electrical braking torque limit based on parameters of the motor but also correction of limitations of previous research are presented based on the regenerative power analysis of permanent magnet synchronous motors (PMSMs) given in [13] and [14].

II. Regenerative Power Analysis for PMSMs

The braking force of electric vehicles consists of two torques: Electrical braking torque and mechanical (friction) braking torque. Since the rated torque of the electric motor is constant and is not sufficient for the electric vehicles to stop in heavy-braking situations, the mechanical torque from the friction braking system is needed to ensure braking performance [15]. Therefore, the electrical braking torque from the motor will only achieve maximum regenerative power at all operating speeds when the mechanical torque is controlled to meet the braking torque requirement. In this section, regenerative power is analyzed for two kinds of PMSMs. Since PMSMs are widely used for the traction motor of electric vehicles, it is reasonable to analyze regenerative power based on their characteristics. Based on a regenerative power analysis, the maximum regenerative power and the maximum regenerative power point (MRPP) for a given speed are calculated for each PMSM using the parameters of that motors. Since the analysis of SPMSM is simpler, the regenerative power analysis is given for SPMSM first, and the analysis for IPMSM is presented based on this. Also, since the copper loss takes the most of the total loss in low-speed operation [16], the regenerative power analysis for low-speed torque limiters only considers the copper loss in this section.

A. Regenerative Power Analysis for SPMSM at a Given Speed

Let us consider the synchronous reference frame voltage equation of SPMSM given in the following equation:

$$\begin{bmatrix} v_d^e \\ v_q^e \end{bmatrix} = \begin{bmatrix} R_s + sL_s & -L_s\omega_e \\ L_s\omega_e & R_s + sL_s \end{bmatrix} \begin{bmatrix} i_d^e \\ i_q^e \end{bmatrix} + \begin{bmatrix} 0 \\ \omega_e\phi_f \end{bmatrix}. \quad (1)$$

Since the dynamic power of the motor changes according to speed if the electrical braking torque is constant, (1) can be modified to (2), considering only an electrical steady state

$$\begin{bmatrix} v_d^e \\ v_q^e \end{bmatrix} = \begin{bmatrix} R_s & -L_s\omega_e \\ L_s\omega_e & R_s \end{bmatrix} \begin{bmatrix} i_d^e \\ i_q^e \end{bmatrix} + \begin{bmatrix} 0 \\ \omega_e\phi_f \end{bmatrix}. \quad (2)$$

Based on (2), the electrical power flowing into the motor can be calculated as follows:

$$\begin{aligned} P_{e\_S} &= \tfrac{3}{2}(v_d^e i_d^e + v_q^e i_q^e)\big|_{i_d=0} \\ &= \frac{3}{2} v_q^e i_q^e \\ &= \frac{3}{2}(R_s i_q^{e2} + \omega_e \phi_f i_q^e). \end{aligned} \quad (3)$$

To minimize the copper loss of the motor, the *d*-axis current of SPMSM should be controlled to be zero and then the active power of SPMSM results in two terms: copper loss, and the dynamic power of the motor. Fig. 2 shows the active power plot based on (3). Since the active power of SPMSM is a summation of second- and first-order polynomials, which are copper loss and dynamic power terms, respectively, it always has a minimum or maximum point at any given speed. Since this point only appears when the copper loss and dynamic power term have a reverse polarity to each other, we can know from four-quadrant operation that this point exists in regenerative braking, and, therefore, there always exists a single *q*-axis current point, which gives the maximum regenerative power for that motor speed.

Fig. 3 shows the active power plot of SPMSM for a given speed. The current maximizing the regenerative power for SPMSM, which will be called the MRPP current for

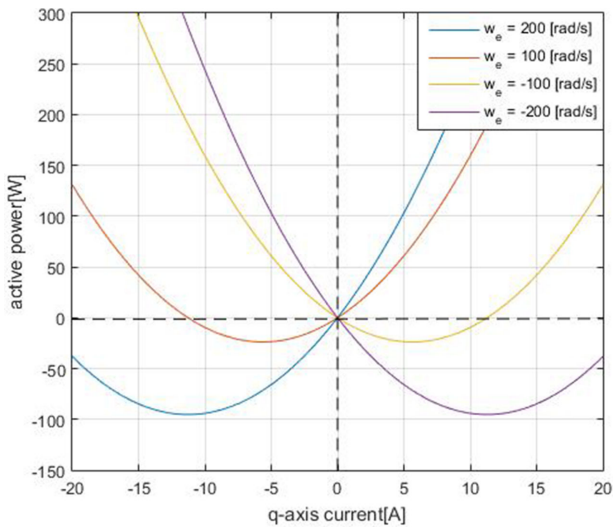

Fig. 2. Active power variation of SPMSM according to q-axis current and motor speed.

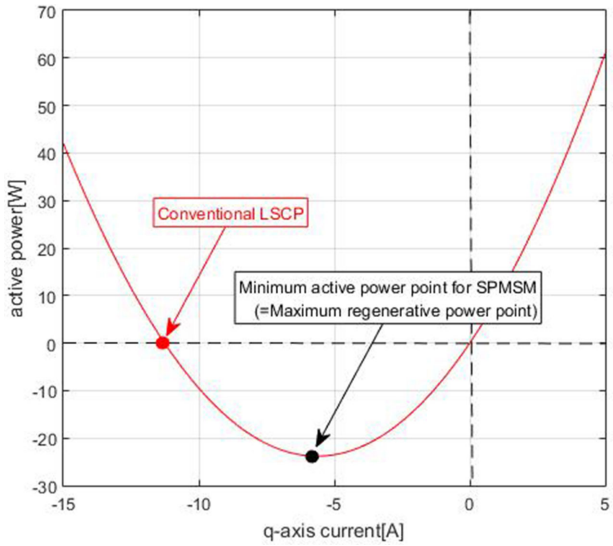

Fig. 3. Active power variation of SPMSM according to q-axis current for a given motor speed.

SPMSM($i^e_{q\_S_{\min}}$), can simply be obtained based on the zero point of the active power slope as in the following equations:

$$\frac{dP_{e\_S}}{di^e_q} = \frac{3}{2}(2R_s i^e_q + \omega_e \phi_f) \tag{4}$$

$$\frac{dP_{e\_S_{\min}}}{di^e_q} = \frac{3}{2}(2R_s i^e_q + \omega_e \phi_f) = 0. \tag{5}$$

Therefore, the MRPP current is calculated as follows:

$$i^e_{q\_S_{\min}}(\omega_e) = -\frac{\phi_f \omega_e}{2R_s}. \tag{6}$$

If the electrical speed of the motor is taken as a variable, shown in (6), the current can be calculated based on the motor speed since it is the only variable in the equation. In summary, the current of SPMSM can regenerate the maximum power when the q-axis current is controlled to be the result of (6).

Additionally, the maximum regenerative power can be calculated by putting (6) into (3) as follows:

$$\begin{aligned} P_{e\_S_{\mathrm{MRPP}}} &= \frac{3}{2}(R_s i^{e2}_{q\_S_{\min}} + \omega_e \phi_f i^e_{q\_S_{\min}}) \\ &= \frac{3}{2}\left(\frac{\phi_f^2 \omega_e^2}{4R_s} - \frac{\phi_f^2 \omega_e^2}{2R_s}\right) \\ &= -\frac{3\phi_f^2 \omega_e^2}{8R_s}. \end{aligned} \tag{7}$$

Also, the exact location of LSCP that is popularly used in conventional studies is shown in Fig. 3. Since the definition of LSCP is the point that the battery current starts to get reversed, the active power of the motor is zero at LSCP and there is an infinite number of LSCP according to the speed of the motor, but none of them gives better regenerative power than MRPP.

Therefore, regenerative braking based on LSCP could never restore the maximum regenerative energy even if dynamic LSCP is estimated without an error.

B. Regenerative Power Analysis for IPMSM for a Given Speed

To define MRPP currents for IPMSM, the same approach is taken as in SPMSM. Equation (8) is the synchronous reference frame voltage equation of IPMSM, and (9) is the same voltage equation but considering a steady state only

$$\begin{bmatrix} v^e_d \\ v^e_q \end{bmatrix} = \begin{bmatrix} R_s + sL_d & -L_q\omega_e \\ L_d\omega_e & R_s + sL_q \end{bmatrix} \begin{bmatrix} i^e_d \\ i^e_q \end{bmatrix} + \begin{bmatrix} 0 \\ \omega_e \phi_f \end{bmatrix} \tag{8}$$

$$\begin{bmatrix} v^e_d \\ v^e_q \end{bmatrix} = \begin{bmatrix} R_s & -L_q\omega_e \\ L_d\omega_e & R_s \end{bmatrix} \begin{bmatrix} i^e_d \\ i^e_q \end{bmatrix} + \begin{bmatrix} 0 \\ \omega_e \phi_f \end{bmatrix}. \tag{9}$$

Equations (8) and (9) are a little different from (1) and (2) because the inductance of the d- and q-axes of the synchronous reference frame are different for IPMSM. Using (9), the active power of IPMSM can be calculated as in the following equation:

$$\begin{aligned} P_{e\_I} &= \frac{3}{2}(v^e_d i^e_d + v^e_q i^e_q) \\ &= \frac{3}{2}(R_s i^{e2}_d + R_s i^{e2}_q + (L_d - L_q)\omega i^e_d i^e_q + \omega_e \phi_f i^e_q). \end{aligned} \tag{10}$$

Since the d-axis current value cannot be assumed to be zero in IPMSM because of the difference in inductance, two more terms appear in (10) than in the result of (3), but the concept of active power remains the same. The first two terms from the result in (10) are copper loss terms and the last two terms represent the dynamic power.

Fig. 4 shows the active power plot of IPMSM. Since there are two variables for currents, the plot is 3-D, while the active power plot for SPMSM is 2-D, as shown in Fig. 2. Although IPMSM and SPMSM have different dimensions for the active power plot; they both have a single minimum/maximum active power point in regenerative braking operation for a given speed as shown in

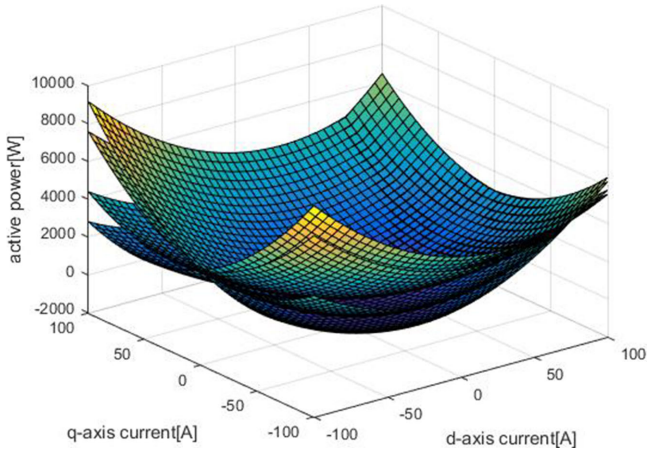

Fig. 4. Active power variation of IPMSM according to q-axis current and motor speed.

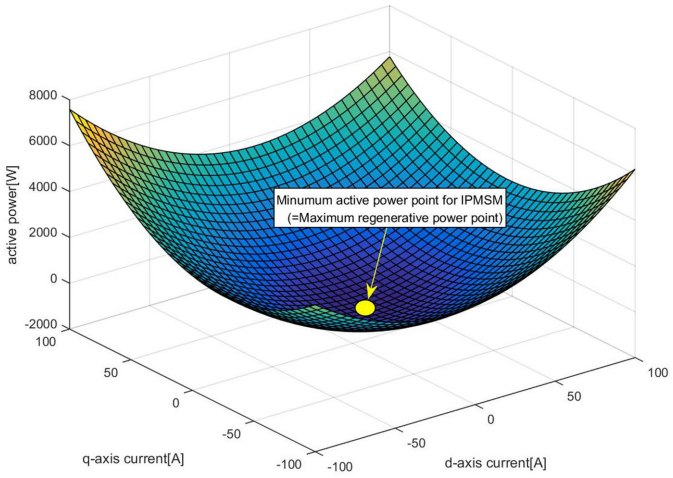

Fig. 5. Active power variation of IPMSM according to q-axis current for a given motor speed.

Figs. 3 and 5. However, the d-axis current has a certain value only for IPMSM. To find the combination of currents that gives maximum regenerative power for IPMSM, the gradient of (10) is obtained as shown in (11), and the slope values are set to zero in (12)

$$\begin{aligned}\frac{\partial P_{e\_I}}{\partial i_d^e} &= \frac{3}{2}(2R_s i_d^e - L_q i_q^e \omega_e + L_d \omega_e i_q^e)\\ \frac{\partial P_{e\_I}}{\partial i_q^e} &= \frac{3}{2}(2R_s i_q^e + L_d i_d^e \omega_e - L_q \omega_e i_d^e + \omega_e \phi_f) \qquad (11)\\ \frac{\partial P_{e\_I_{\min}}}{\partial i_d^e} &= \frac{3}{2}(2R_s i_d^e - L_q i_q^e \omega_e + L_d \omega_e i_q^e) = 0\\ \frac{\partial P_{e\_I_{\min}}}{\partial i_q^e} &= \frac{3}{2}(2R_s i_q^e + L_d i_d^e \omega_e - L_q \omega_e i_d^e + \omega_e \phi_f) = 0.\end{aligned} \qquad (12)$$

Based on (12), the d-/q-current combination for MRPP can be calculated as in the following equation:

$$\begin{aligned}i_d^e(\omega_e, i_q^e) &= -\frac{(L_d - L_q)\omega_e i_q^e}{2R_s}\\ i_q^e(\omega_e, i_d^e) &= -\frac{(L_d - L_q)\omega_e i_d^e + \omega_e \phi_f}{2R_s}.\end{aligned} \qquad (13)$$

To eliminate the cross-coupling component for both current equations in (13), the q-axis current equation is put into the d-axis current equation in (13) and vice versa, and then the result is as shown in the following equation:

$$\begin{aligned}i_{d\_I_{\min}}^e(\omega_e) &= \frac{(L_d - L_q)\omega_e^2 \phi_f}{4R_s^2 - (L_d - L_q)^2 \omega_e^2}\\ i_{q\_I_{\min}}^e(\omega_e) &= \frac{-2R_s \omega_e \phi_f}{4R_s^2 - (L_d - L_q)^2 \omega_e^2}.\end{aligned} \qquad (14)$$

As you can see, the MRPP currents for IPMSM can also be defined based on only the speed of the motor, and for each speed, there is a single MRPP. Even though it looks complicated, the calculation is very simple because each parameter, besides speed, is constant. Also, the result of MRPP currents for IPMSM shown in (14) is different from currents for SPMSM shown in (6); the MRPP currents need to be generalized for all kind of PMSMs to simplify the follow-up process. Since the only difference between (14) and (6) are the inductance values, we can try to put the characteristics of SPMSM into (14) as follows:

$$\begin{aligned}i_{d\_I_{\min}}^e(\omega_e)\big|_{L_d = L_q} &= 0 = i_{d\_S_{\min}}^e(\omega_e)\\ i_{q\_I_{\min}}^e(\omega_e)\big|_{L_d = L_q} &= -\frac{\phi_f \omega_e}{2R_s} = i_{q\_S_{\min}}^e(\omega_e).\end{aligned} \qquad (15)$$

Since the outcome of (15) is the same as the MRPP currents for SPMSM, the MRPP currents for all types of PMSM can be generalized by (14) as follows:

$$\begin{aligned}i_{d\_\mathrm{MRPP}}^e(\omega_e) &= i_{d\_I_{\min}}^e(\omega_e) = \frac{(L_d - L_q)\omega_e^2 \phi_f}{4R_s^2 - (L_d - L_q)^2 \omega_e^2}\\ i_{q\_\mathrm{MRPP}}^e(\omega_e) &= i_{q\_I_{\min}}^e(\omega_e) = \frac{-2R_s \omega_e \phi_f}{4R_s^2 - (L_d - L_q)^2 \omega_e^2}.\end{aligned} \qquad (16)$$

Using the generalized MRPP currents, regenerative power can also be generalized as in the following equation:

$$\begin{aligned}P_{e\_\mathrm{MRPP}} = \frac{3}{2}(&R_s i_{d\_\mathrm{MRPP}}^{e2} + R_s i_{q\_\mathrm{MRPP}}^{e2}\\ &+ \omega_e \phi_f i_{q\_\mathrm{MRPP}}^e\\ &+ (L_d - L_q)\omega i_{d\_\mathrm{MRPP}}^e i_{q\_\mathrm{MRPP}}^e).\end{aligned} \qquad (17)$$

If you put the conditions from SPMSM($L_d = L_q$) in (17), you will get the same result as (7). Besides, in the case of IPMSM, the LSCP is given as a line and not a point since there is an infinite combination of currents that give an active power of zero for a given motor speed, as shown in Fig. 5. However, there is only a single LSCP the user can reach for a given speed that depends on the torque control scheme used; this will be covered in the next section.

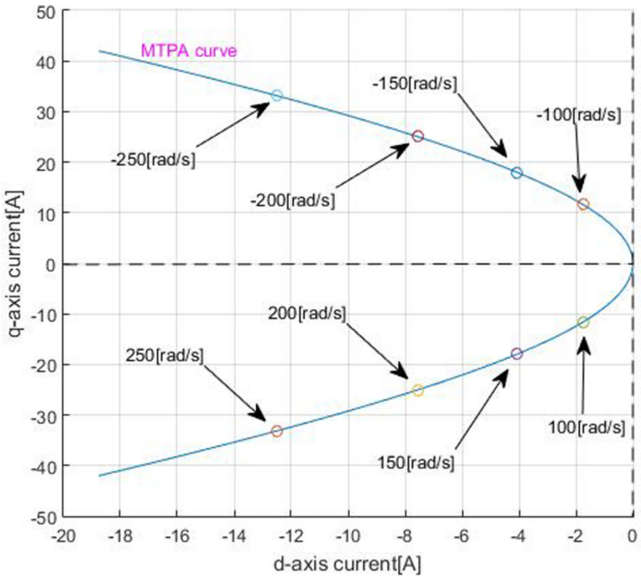

Fig. 6. Relationship between MRPP currents and MTPA curve in IPMSM.

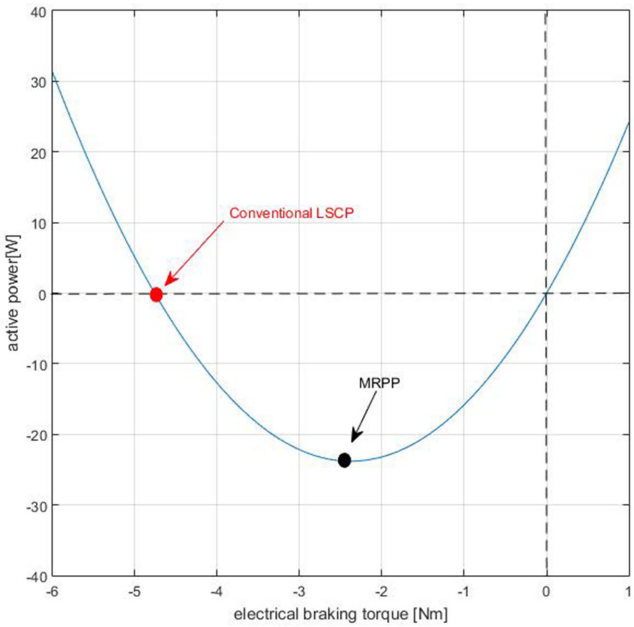

Fig. 7. SPMSM active power variation according to the electrical braking torque at a given speed.

C. MRPP Torque Calculation

The generalized MRPP currents($i^e_{d\_\mathrm{MRPP}}, i^e_{q\_\mathrm{MRPP}}$) in (16) are clear and easy to implement, but, in the case of IPMSM, if the magnitude of the current reaches the current limit, it becomes hard to process because the d- and q-axis currents are calculated separately. Also, since the electrical braking force is normally given as a form of electrical braking torque reference and the dynamics of the braking system are analyzed based on the torque, it would be easier to implement and understand if the MRPP is given as a torque value.

Fig. 6 shows the combination of MRPP currents of IPMSM at a few different points of speed. As mentioned earlier, the current for SPMSM is on the q-axis, but the MRPP currents for IPMSM appear to be at a certain point on the maximum torque per ampere (MTPA) curve. This is due to the same reason as the SPMSM having the MRPP current in the q-axis, that is, to have the maximum dynamic power with the minimum copper loss. Therefore, the MRPP torque can be defined as a certain point on the MTPA torque curve ($T_{e\_\mathrm{MRPP}} \in T_{\mathrm{MTPA}}$).

Consequently, the electrical braking torque can simply be calculated by putting those combinations of currents into the torque equation for PMSM shown in the following equation:

$$T_e = \frac{P}{2}\frac{3}{2}(\phi_f i^e_q + (L_d - L_q) i^e_d i^e_q). \tag{18}$$

In (18), only q-axis current is applied for SPMSM and current combinations that match the MTPA torque are used for IPMSM.

Figs. 7 and 8 show the MTPA torque and power characteristic of PMSMs for a given speed. In the case of SPMSM shown in Fig. 7, the plot is similar to Fig. 3 because only q-axis current decides the electrical braking torque. However, for IPMSM shown in Fig. 8, the characteristics are much simpler than that in Fig. 5 and, therefore, easier to implement and comprehend.

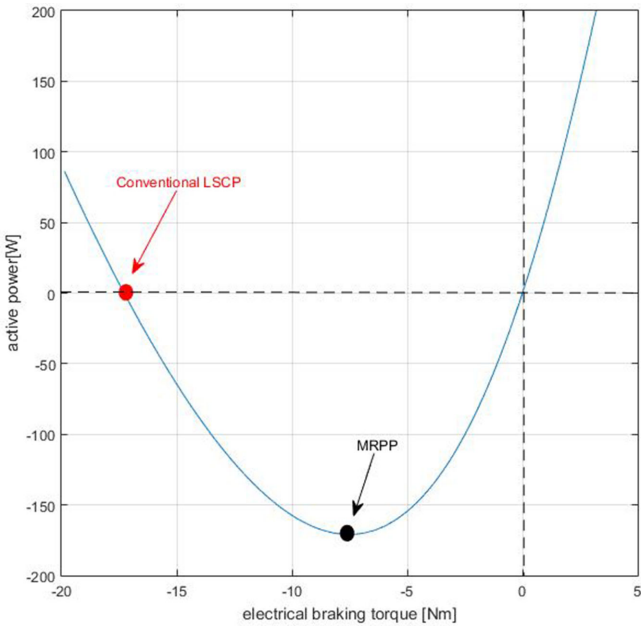

Fig. 8. IPMSM active power variation according to the electrical braking torque at a given speed.

Also, the LSCP is given as a single value of the torque for both types of PMSMs in this figure, and it is obvious that neither SPMSM nor IPMSM can ever reach the maximum regenerative power.

To obtain a MRPP torque based on motor speed, the MRPP currents from (16) are put into (18). Due to the differences in characteristics of SPMSM and IPMSM, the MRPP torques are

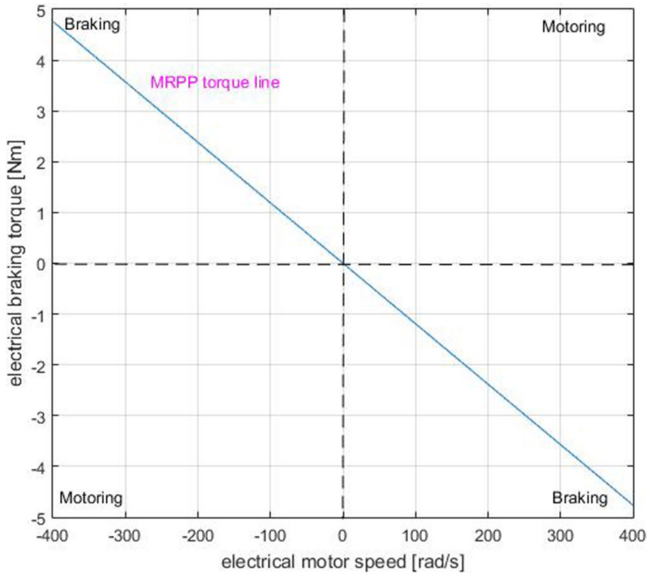

Fig. 9. MRPP line for SPMSM in four-quadrant operation.

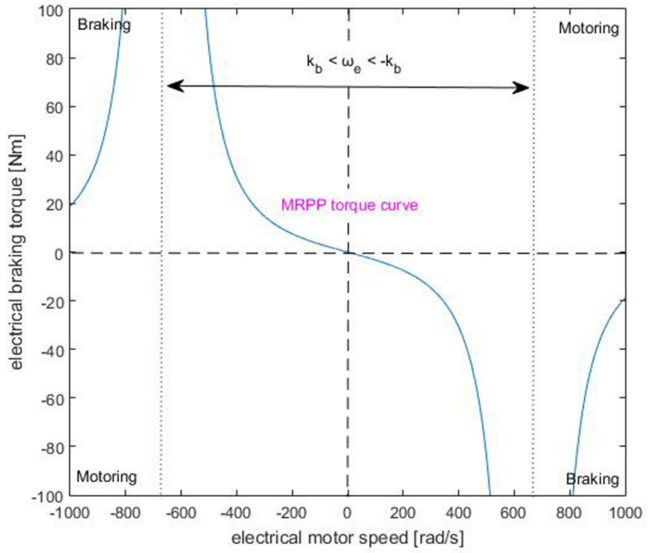

Fig. 10. MRPP curve for IPMSM in four-quadrant operation.

calculated separately as follows:

$$T_{e\_\mathrm{MRPP}}(\omega_e)\big|_{L_d=L_q} = -\frac{3}{8R_s}\phi_f^2 P\omega_e$$

$$T_{e\_\mathrm{MRPP}}(\omega_e)\big|_{L_d\neq L_q} = -\frac{3k_b^4\phi_f^2 P}{8R_s}\frac{\omega_e}{(\omega_e+k_b)^2(\omega_e-k_b)^2}$$

$$\left(\text{where} k_b = \frac{2R_s}{L_d-L_q}\right). \tag{19}$$

Figs. 9 and 10 show the MRPP torque and speed plot for SPMSM and IPMSM. Since the MRPP torque for SPMSM is proportional to the negative of speed in (19), the MRPP torque decreases as speed increases, as shown in Fig. 9. However, as shown in Fig. 10, the MRPP torque of IPMSM goes to infinity

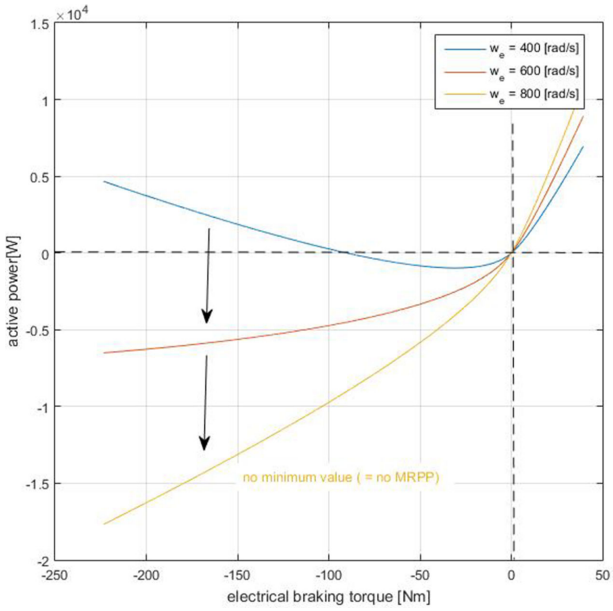

Fig. 11. Change of IPMSM torque–power characteristic as the motor speed exceeds k_b.

as speed increases and then becomes a large negative value past a certain point. This implies that if the absolute value of the motor speed exceeds the absolute value of k_b ($|\omega_e| > |k_b|$), the physical meaning of the equation is changed from representing the MRPP to having no physical real-world meaning. In other words, the calculated MRPP torque for IPMSM is only valid when $k_b < \omega_e < -k_b$, and outside of these bounds ($\omega_e > -k_b$ and $\omega_e < k_b$), more electrical braking torque results in more regenerative power because there is no maximum point for regenerative power in these conditions, as shown in Fig. 11.

III. Proposed Torque Limit Trajectory for Regenerative Braking

Based on the regenerative power analysis given in the previous section, electrical braking torque limiters are designed for PMSM drives. To design the proper electrical braking torque limit trajectory, two principles are followed.

1) The braking torque should not invade the motoring operation region.
2) Increases in electrical braking torque should only result in increases of regenerative power.

The second principle can also be expressed by the following equation:

$$\begin{cases} \frac{dP_e}{dT_e} > 0, \text{ if } \omega_e > 0 \\ \frac{dP_e}{dT_e} < 0, \text{ if } \omega_e < 0. \end{cases} \tag{20}$$

Fig. 12 shows the MTPA torque and power characteristic for IPMSM for the speeds given in Fig. 8, which includes the characteristics of SPMSM as well, with the two principles above. As shown in this figure, the torque values that regenerate power to charge the battery are from zero to LSCP; if the torque has any other values, power is dissipated. Also, since the slope of

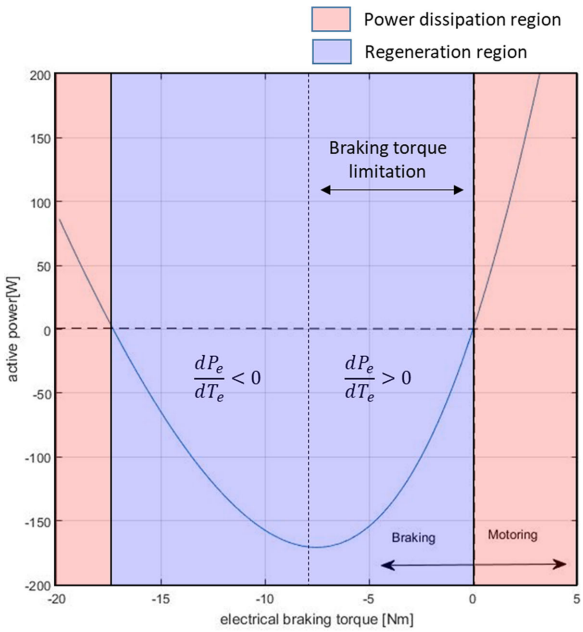

Fig. 12. IPMSM electrical braking torque limitation for a given speed.

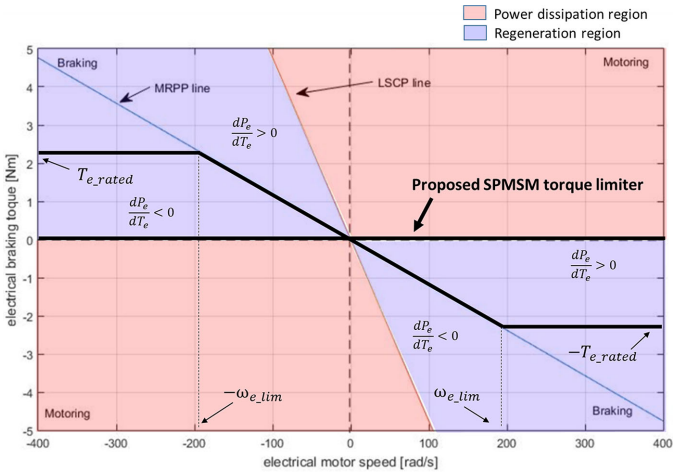

Fig. 13. Proposed SPMSM torque limiter based on MRPP torque.

the power is changing according to the value of MRPP torque, regenerative power increases along with the electrical braking torque only if the absolute value of torque is smaller than the MRPP torque in the regeneration region. Therefore, the electrical braking torque should be limited from zero to the MRPP torque to meet the requirements shown in Fig. 12.

A. Torque Limit Trajectory for SPMSM

In Fig. 13, the torque limit trajectory for SPMSM is presented based on the MRPP torque equation, (19), for SPMSM and the principles given above. As shown in this figure, the power is dissipated in all motoring and braking operation where the electrical braking torque exceeds the LSCP line. Also, the gradient of the MRPP torque curve is changed in the regeneration region if the torque exceeds the MRPP line. Therefore, during

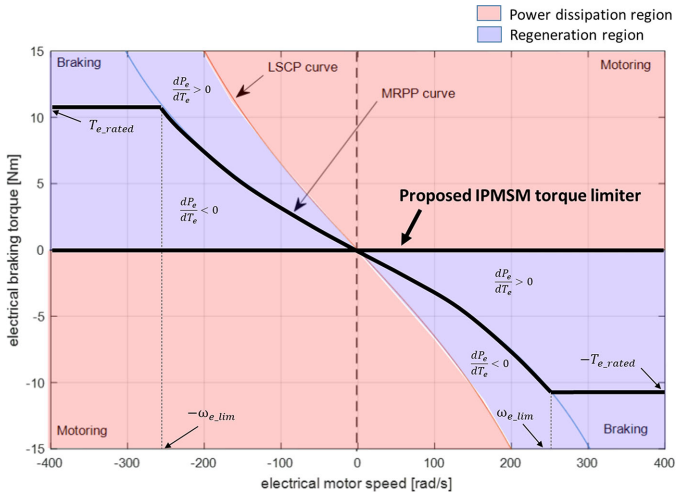

Fig. 14. Proposed IPMSM torque limiter based on MRPP torque.

regenerative braking of the SPMSM drive, a limiter should restrict the electrical braking torque from zero to the MRPP line, as shown in Fig. 13, to maximize the performance of the vehicle.

Additionally, since the calculated MRPP torque value in high-speed operation could be so high that it makes the microprocessor malfunction due to problems such as data overflow, it is important to find the speed where MRPP torque reaches the rated torque of the motor so that the MRPP torque calculation can be disabled if the motor speed exceeds this value for secure operation. This motor speed is called the limit speed (ω_{e_lim}) in this article and is shown in Fig. 13.

The limit speed for SPMSM can be calculated as shown in (21) and (22) based on the MRPP torque equation, (19), for SPMSM with the rated torque

$$T_{e\_\mathrm{rated}}\big|_{L_d=L_q} = -\frac{3}{8R_s}\phi_f^2 P\omega_{e\_\mathrm{lim}} \tag{21}$$

$$\omega_{e\_\mathrm{lim}} = -\frac{8R_s}{3\phi^2 P}T_{e\_\mathrm{rated}}. \tag{22}$$

B. Torque Limit Trajectory for IPMSM

Fig. 14 shows the torque limit trajectory based on the MRPP torque for IPMSM from (19) and the two principles mentioned above. In the same way as the limiter for SPMSM, power dissipates in all motoring and braking operations when the torque is above the LSCP line. Also, the gradient of the power curve changes if the torque exceeds the MRPP torque in the braking region. Even though the MRPP torque line for IPMSM is not linear, there is no extra procedure required in this case as the torque limit trajectories for both PMSMs are based on the calculation presented in (19).

Since the MRPP torque for IPMSM goes to infinity as the speed increases, it is essential for IPMSMs to identify the limit speed and disable the MRPP torque calculation when the speed exceeds it to prevent microprocessor malfunction. The limit

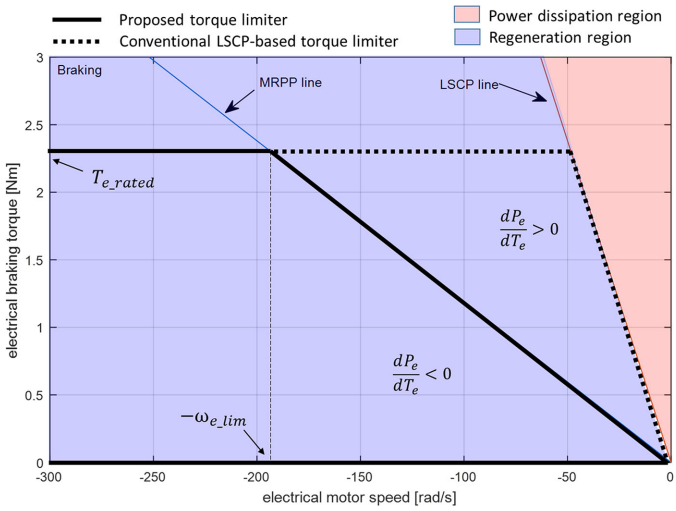

Fig. 15. Comparison between conventional and the proposed toque limiter for SPMSM.

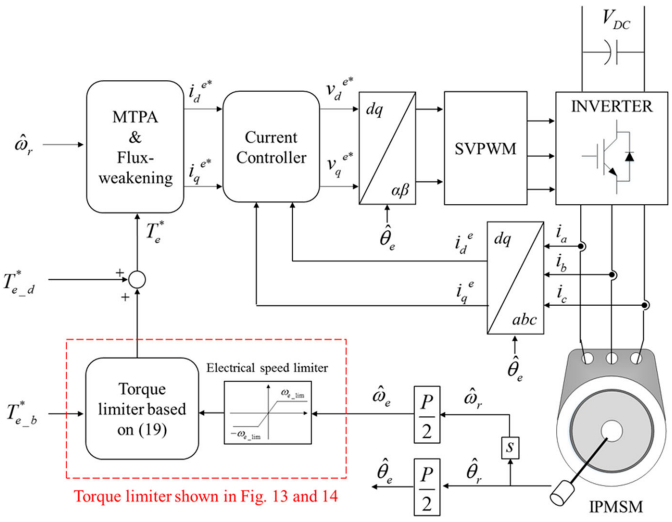

Fig. 16. Block diagram of implementation of the proposed torque limiter.

speed for IPMSM can be calculated as follows.

$$T_{e\_\mathrm{rated}}\big|_{L_d \neq L_q} = -\frac{3k_b^4\phi_f^2 P}{8R_s}\frac{\omega_{e\_\mathrm{lim}}}{(\omega_{e\_\mathrm{lim}}+k_b)^2(\omega_{e\_\mathrm{lim}}-k_b)^2} \left(\text{where, } k_b = \frac{2R_s}{L_d - L_q}\right) \tag{23}$$

$$\omega_{e\_\mathrm{lim}}^4 - 2k_b^2\omega_{e\_\mathrm{lim}}^2 - \frac{3k_b^4\phi_f^2 P}{8RT_{e\_\mathrm{rated}}}\omega_{e\_\mathrm{lim}} + k_b^2 = 0. \tag{24}$$

Even though there are multiple solutions to (24), only one solution is valid and this solution gives the minimum absolute value in the braking region of four-quadrant operation by considering the given rated torque (T_{e_rated}).

C. Torque Limiter Interpretation of Conventional LSCP-Based Regenerative Braking

In the previous sections, it is consistently mentioned that a torque limit based on LSCP could never achieve maximum regenerative power and so torque limit trajectories proposed for both PMSMs are based on MRPP instead. To make fair and precise comparisons, the torque limit interpretation of a dynamic LSCP-based regenerative braking technique is given at its peak performance with the proposed torque limiter.

Fig. 15 shows a comparison between the proposed SPMSM torque limiter and the torque limiter interpretation of a regenerative braking technique based on dynamic LSCP. While the proposed torque limiter follows the MRPP torque line in low-speed operation, the torque limit trajectory for a conventional torque limiter follows the LSCP line because the dynamic LSCP used is assumed to be perfectly identified. In high-speed operation, the operating speed is above the limit speed and the proposed and conventional LSCP-based torque limiters have the same performance since torque is limited to the rated torque in this region and is the same for both approaches. However, in low-speed operation, the speed is below the limit speed, so conventional LSCP invades the region where increased braking torque results in a decrease of regenerative power in the regeneration region. This causes less regenerative power to be harvested with a conventional torque limiter during rapid braking since the regenerative power is higher when less electrical braking torque is used in this region. Therefore, even though the difference of regenerative power between conventional and the proposed torque limiter for one braking situation is not relatively high because it occurs in low-speed operation, the total regenerative energy difference would not be insignificant considering long driving times, and the difference would be even more significant in heavy stop-and-go traffic.

D. Implementation of the Proposed Torque Limiter

Fig. 16 shows the simple block diagram for the implementation of the proposed torque limiter. Since the proposed method modifies the torque reference only, any conventional current (torque) control method can be used as long as there is no steady-state error. The torque reference is calculated by adding the driving and braking torques (T_{e_d} and T_{e_b}), and the proposed torque limiter is only applied for the braking torque. For the proposed torque limiter, the electrical motor speed with speed limiter is used to make the torque limiter shown in Figs. 13 and 14.

However, as implied in (19), the proposed torque limiter is highly dependent on motor parameters (L_{dq}, ϕ_f, R_s). Since the non-linear behavior of the motor is causing parameter variation, it should be considered in real-world applications to maximize the regenerative energy with the proposed torque limiter. Since implementation based on 3-D lookup table (3-D-LUT), in which index values are torque, speed, and temperature of the motor, is the most popular parameter variation compensation method for the MTPA torque control, in Fig. 17, the proposed braking torque limiter implementation with 3-D-LUT based MTPA torque controller is given as an example.

Since MRPP currents are always on the MTPA curve as shown in Fig. 6, the output of the torque limit table can be the input

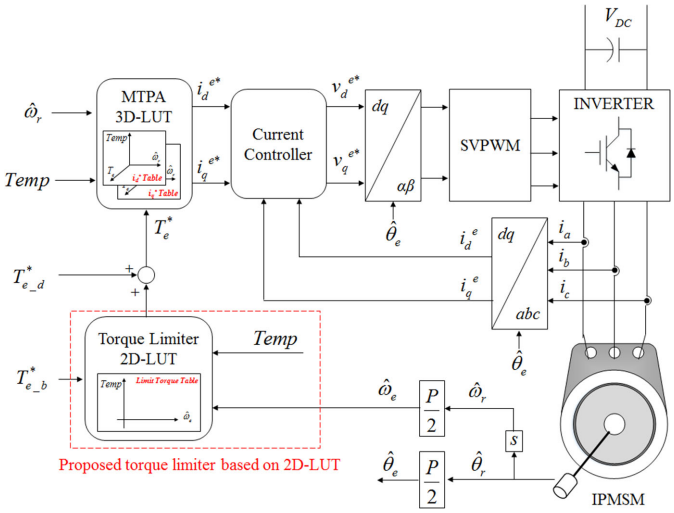

Fig. 17. Block diagram of lookup-table-based implementation of the proposed torque limiter.

of the MTPA table. In this way, the L_{dq} variation from the saturation effect does not have to be considered in the torque limit table since it is compensated in the MTPA table. However, ϕ_f and R_s variation from the various operating temperatures should be considered since MRPP currents can move back and forth on the MTPA curve according to the operating temperature. Therefore, additional 2-D-LUT, in which index values are speed and temperature of the motor, should be made for torque limiter table for the proposed braking torque limiter, and the torque limit value written in the table can simply be the electrical braking torque value that has the maximum regenerative power for the corresponding speed and temperature of the motor. Although the limit speed (ω_{e_lim}) is also changing according to the parameter variation according to (22) and (24), calculation of ω_{e_lim} does not have to be done in the table-based implementation because the limit torque in the table cannot be an infinite value.

IV. Simulation

To verify the proposed braking torque limiter and its related analysis in the previous sections, a MATLAB-based simulation is performed. Table I shows the parameters of PMSMs used for this simulation. Based on the given parameters, the proposed torque limiter is built and its regenerative power is compared with conventional regenerative braking methods.

Figs. 18 and 19 show the MATLAB-based simulation results for PMSM drive systems without a low-speed torque limiter, where the electrical braking torque is always limited to the rated torque of the motor. For comparison, the initial rotor speeds of the simulation for SPMSM and IPMSM are set to 500 and 2500 r/min, respectively. The electrical motor speeds for these initial speeds are 262 and 1047 rad/s, respectively, which are higher than the respective limit speeds of the motors, 201 and 883 rad/s, calculated by (22) and (24). Also, the braking electrical torque values are set to the maximum values for the corresponding braking method and motor parameters considering a rapid braking situation to visualize the differences of

TABLE I
Parameters of PMSMs for Simulation and Experiment

SPMSM	
Rated power	0.75 $[kW]$
Rated speed	3000 $[rpm]$
Maximum speed	6000 $[rpm]$
Rated voltage	200 $[V]$
Rated torque (T_{e_rated})	2.49 $[Nm]$
Stator resistance (R_s)	1.0 [Ω]
d-axis stator inductance (L_s)	2080 $[\mu H]$
q-axis stator inductance (L_s)	2080 $[\mu H]$
Number of poles	10
Rotor flux (ϕ_f)	0.056 [Wb]
IPMSM	
Rated power	6 $[kW]$
Rated speed	4000 $[rpm]$
Maximum speed	10000 $[rpm]$
Rated voltage	200 $[V]$
Rated torque (T_{e_rated})	14.2 $[Nm]$
Stator resistance (R_s)	0.6 [Ω]
d-axis stator inductance (L_d)	303 $[\mu H]$
q-axis stator inductance (L_q)	907 $[\mu H]$
Number of poles	8
Rotor flux (ϕ_f)	0.046 [Wb]

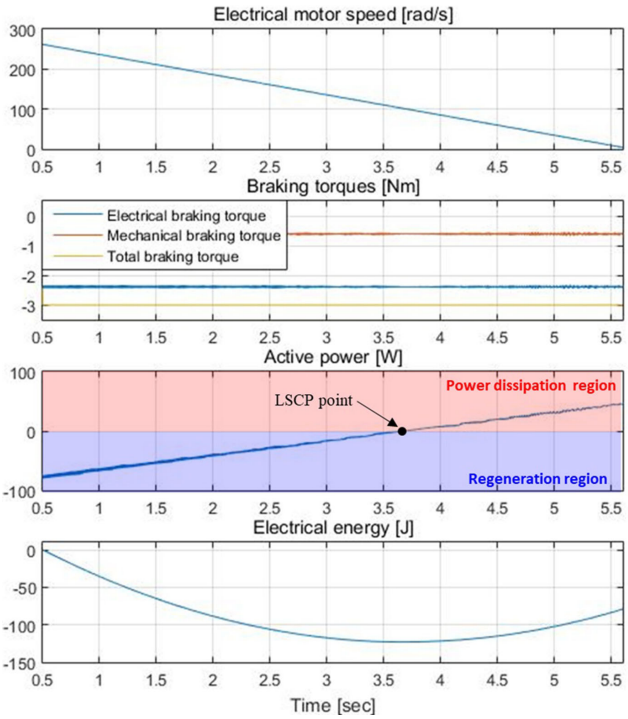

Fig. 18. Simulation results of braking for SPMSM without low-speed electrical torque limiter.

regenerative power and energy in one isolated braking situation. Besides, since mechanical braking torque secures braking performance, the mechanical braking torque should always make up the difference between demanded torque and electrical braking torque. In this simulation, external torque is added to imitate this mechanical braking system and the mechanical torque is shown in the torque waveform from Figs. 18 and 19 along

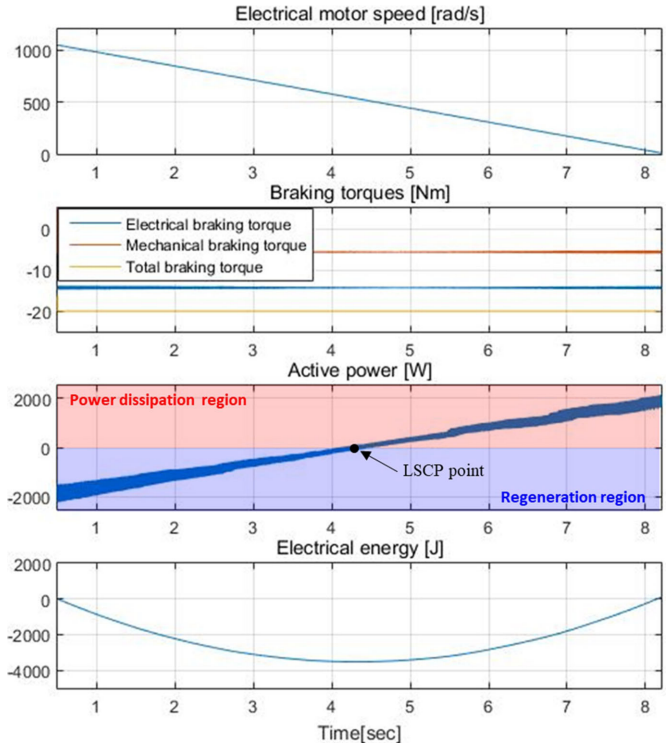

Fig. 19. Simulation results of braking for IPMSM without low-speed electrical torque limiter.

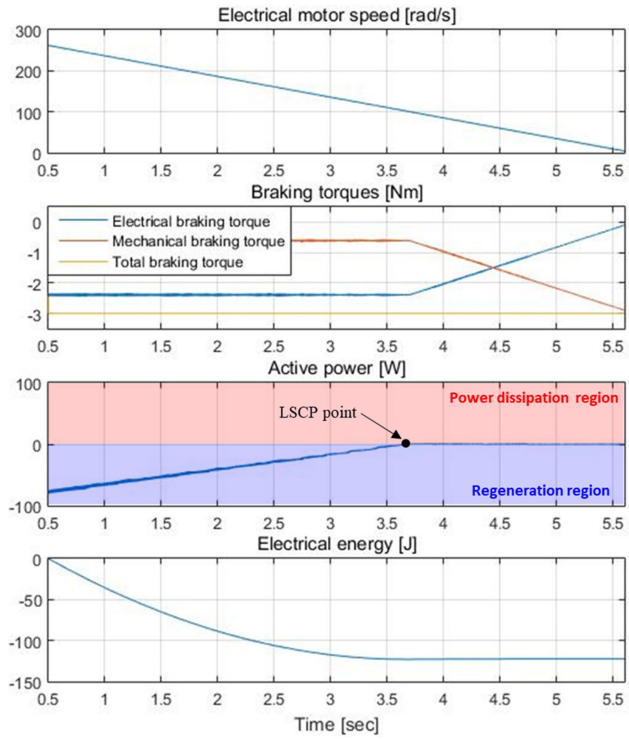

Fig. 20. Simulation results of conventional LSCP-based braking for SPMSM.

with the electrical braking and total torque. As shown in those torque waveforms, the electrical braking torque values for both PMSMs remains constant and results in active power dissipation for PMSMs below the LSCP speed point. This phenomenon causes energy loss from the battery, which is represented as an increment of electrical energy to the motor in Figs. 18 and 19.

In Figs. 20 and 21, results from the simulated conventional dynamic LSCP-based regenerative braking are shown. The speed profiles for both simulations are the same as the ones in Figs. 18 and 19, respectively, so it can be seen that the total braking torque values are the same for both cases. Using this conventional regenerative braking method, the torque values are controlled from certain speeds so that the active power can never have a positive value which indicates that power dissipation will occur during regenerative braking. Therefore, the electrical energies in Figs. 20 and 21 do not change if the torque values start to be controlled, resulting in lower total electrical energies and more regenerative energy than that for the conventional methods shown in Figs. 18 and 19. The simulation results for the proposed MRPP-based regenerative braking are shown in Figs. 22 and 23. Since the maximum electrical braking torque of the PMSM is controlled if the motor speed is below the limit speed in the proposed braking method, the torque changes when the speed decreases below 201 rad/s for SPMSM and below 883 rad/s for IPMSM. Also, electrical torque values are controlled based on the MRPP curves given in the previous section, and, therefore, the LSCP points do not exist in the active power waveform unlike for the other braking methods. In addition, the active power in the proposed method is always a negative value and so is

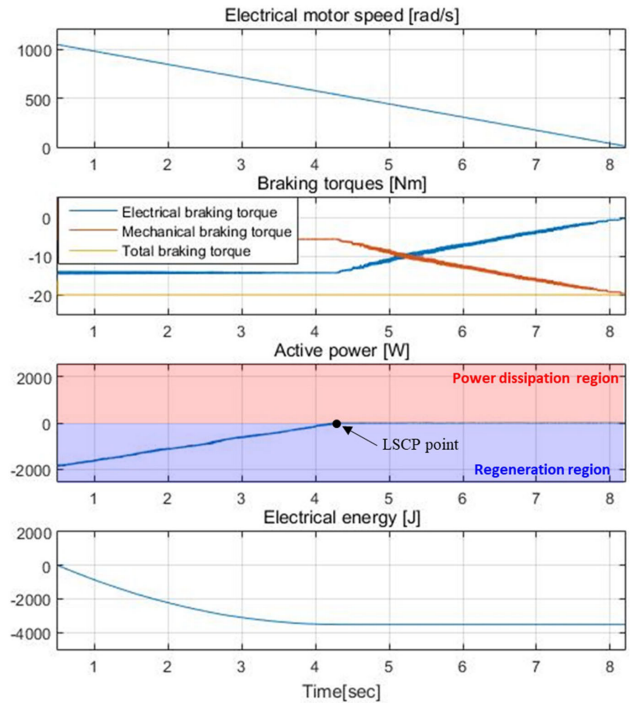

Fig. 21. Simulation results of conventional LSCP-based braking for IPMSM.

regenerating energy for the whole speed range of the motor, and, therefore, the total electrical energies of the proposed braking methods are the smallest among all the braking methods and achieve the maximum regenerative energy.

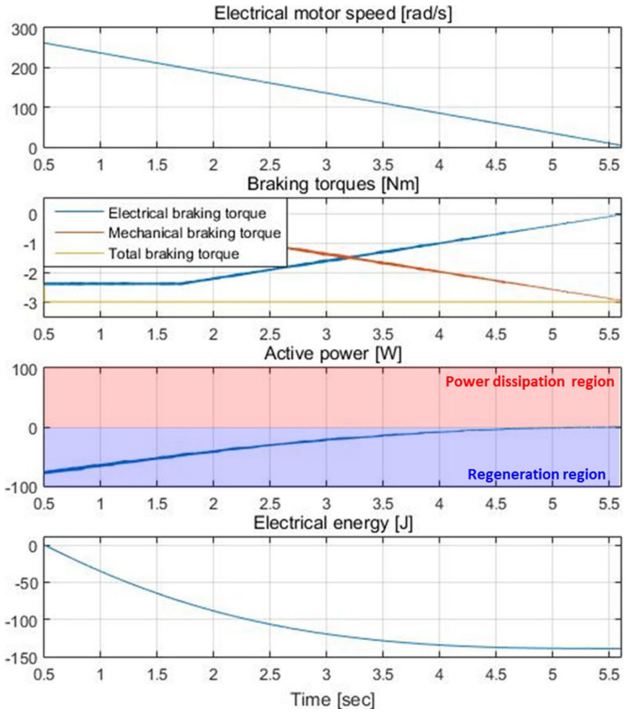

Fig. 22. Simulation results of the proposed MRPP-based braking for SPMSM.

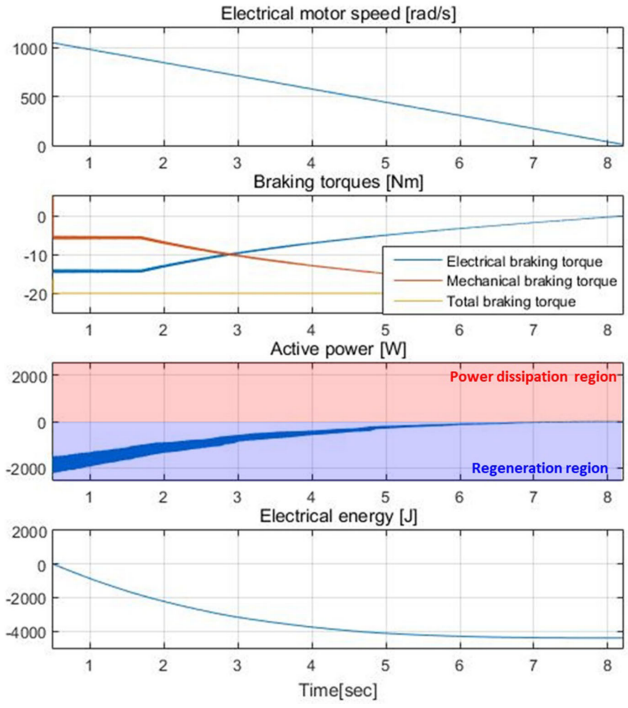

Fig. 23. Simulation results of the proposed MRPP-based braking for IPMSM.

For proper comparison, the torque, active power, and electrical energy of the discussed methods are compared for SPMSM and IPMSM in Figs. 24 and 25, respectively.

For both SPMSM and IPMSM, the active power and electrical energy of the proposed braking methods are the smallest even though the braking torque is also the smallest. This is because

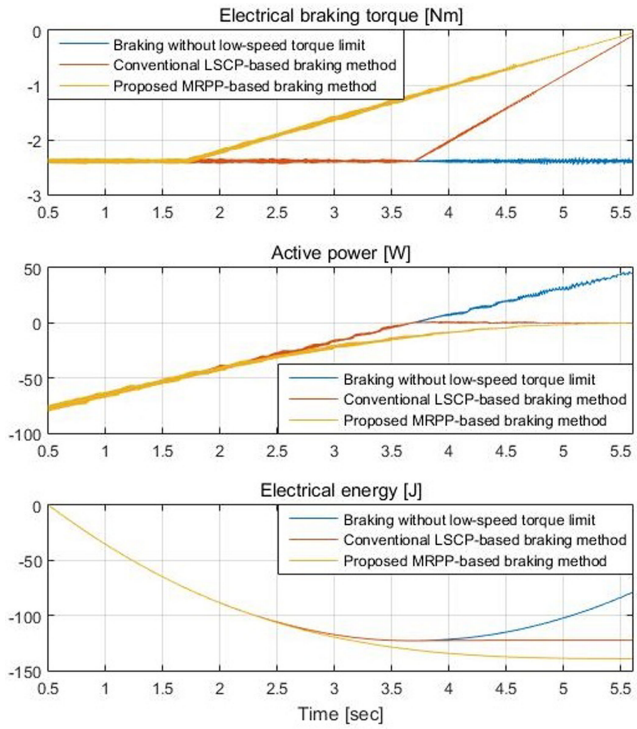

Fig. 24. Electrical braking torque, active power, and energy comparison of the braking methods for SPMSM based on the simulation results.

the two conventional methods violate the second principle of braking torque trajectory, given in Section III, and they are in the region where an increase of braking torque results in a decrease of regenerative power. This also explains why conventional LSCP-based braking methods result in more regenerative power and energy than braking methods without a low-speed torque limit. Additionally, the total amount of regenerated energy for IPMSM is bigger than that for SPMSM. The reason for this is that IPMSM has longer braking times and bigger rated torque even though stator resistance is smaller. In conclusion, the proposed method is more effective for motor drive systems with high inertia and rated torque, which perfectly matches the load and motor characteristics of electric vehicles.

V. Experimental Results

In this section, the implementation of the braking methods is discussed and the experimental results are compared to simulation results to find out whether they are consistent or not. Fig. 26 shows the overall experimental configuration. To simulate a certain motor speed, motor–generator (M-G) sets are configured for both SPMSM and IPMSM. Fig. 27 shows the detailed configuration of M-G set for IPMSM shown in Fig. 26 from a different angle. As shown in this figure, the torque transducer is connected between the IPMSM and the load motor to measure the electrical torque. Also, the active power is calculated based on measured phase currents of PMSMs and the output voltage of the inverter. Since the simulation is based on parameters of actual PMSMs, the parameters from Table I are used for this experiment. The initial speed of the SPMSM is also kept at 500 r/min, but the

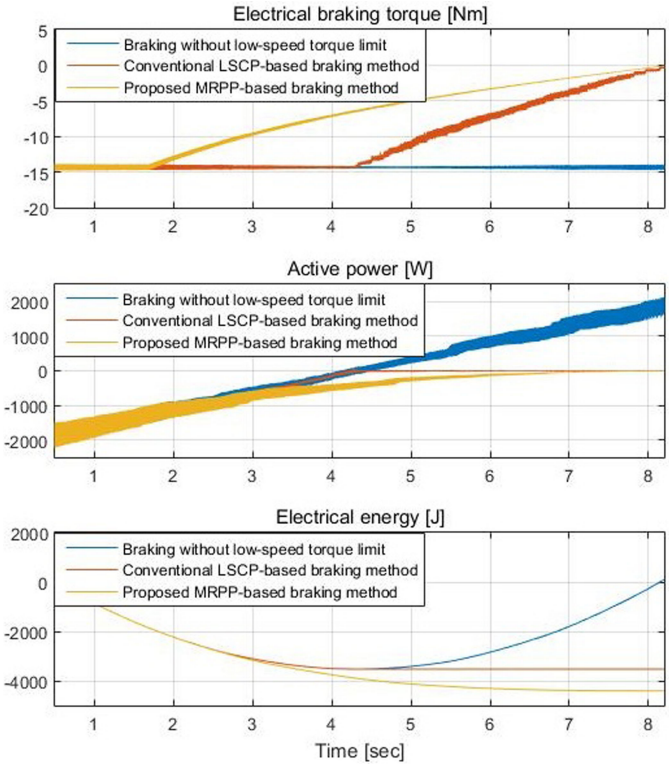

Fig. 25. Electrical braking torque, active power, and energy comparison of the braking methods for IPMSM based on the simulation results.

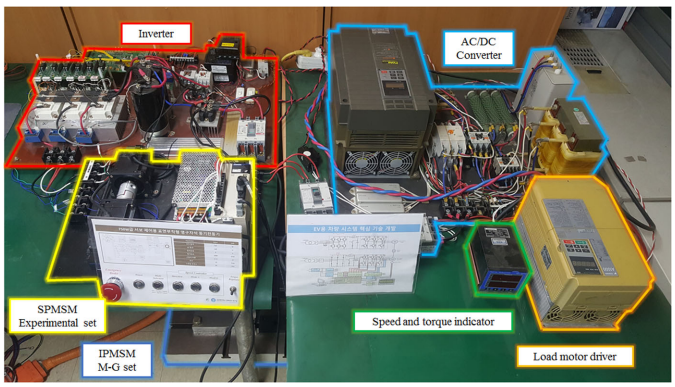

Fig. 26. Experimental configuration.

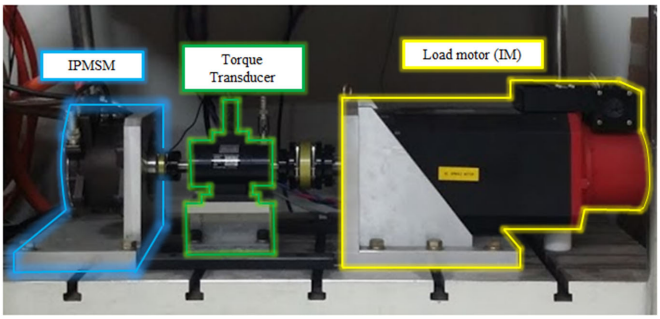

Fig. 27. Detailed experimental configuration of M-G set for IPMSM.

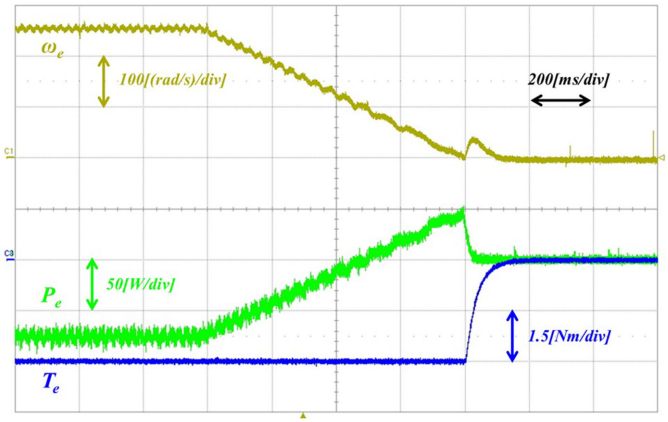

Fig. 28. Experimental results of braking for SPMSM without low-speed electrical torque limiter.

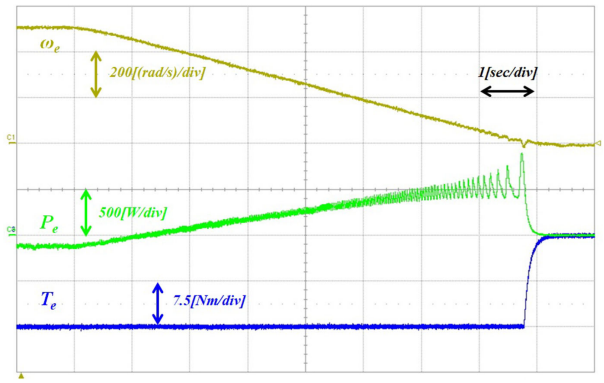

Fig. 29. Experimental results of braking for IPMSM without low-speed electrical torque limiter.

initial speed for IPMSM is adjusted to 1250 r/min because of hardware limitations. For each PMSM, a load motor is connected to the PMSM to control rotor speed, imitating the constant total braking torque and high inertia condition of the simulation.

Figs. 28 and 29 show the experimental results of the braking for PMSMs without low-speed torque limitation. The electrical motor speed (ω_e), active power (P_e), and the electrical braking torque (T_e) are captured and expressed as symbols. In the results for SPMSM shown in Fig. 28, electrical speed of the motor decreases from 262 rad/s, 500 r/min rotor speed, and the electrical braking torque does not change from the rated torque until the motor is stopped. Since the actual inertia of the coupled motor and load in the hardware of SPMSM is very small, there are small oscillations of the speed of the motor, and the speed momentarily changes when electrical braking torque decreases rapidly. However, this phenomenon does not affect the results much and the results are very similar to the simulation results shown in Fig. 18. The experimental results for IPMSM, shown in Fig. 29, seem a bit different from the simulation results, shown in Fig. 19, because the initial speed of the experiment is half that of the simulation. Therefore, the experimental results for IPMSM should be compared with half the simulation results for proper comparison, and when it is done, the results are very similar.

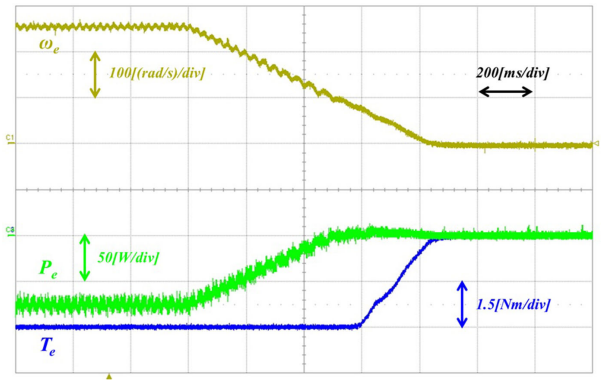

Fig. 30. Experimental results of conventional LSCP-based braking for SPMSM.

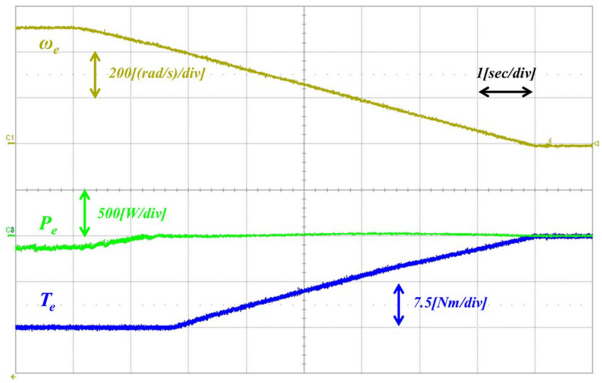

Fig. 31. Experimental results of conventional LSCP-based braking for IPMSM.

In Figs. 30 and 31, a conventional LSCP-based braking method is implemented and tested for PMSMs. Since the motor speed is controlled by the load motor, the speed profiles for both SPMSM and IPMSM are the same no matter which braking method is used. Using this braking method for both PMSMs, the absolute value of the electrical braking torque starts to decrease preventing the active power having a positive value. These results are very similar to the simulation results for conventional LSCP-based braking shown in Figs. 20 and 21. Also, in the results for SPMSM shown in Fig. 30, there is no instantaneous speed change when electrical braking torque is controlled because the torque is gradually decreasing.

The experimental results for the implementation of the proposed MRPP-based braking method is shown in Figs. 32 and 33. As shown in these figures, the torque values are controlled according to their respective MRPP curves causing negative active power to come from the motor for all speeds until the motor is stopped. Since the initial electrical motor speed for IPMSM is 524 rad/s in the experiment, which is smaller than the limit speed of 883 rad/s for IPMSM, the electrical torque of the proposed method for IPMSM is controlled from the beginning, as shown in Fig. 33. Except for this difference, the results of the proposed braking method are the same as those for the simulation shown in Figs. 22 and 23, resulting in maximum regenerative power being achieved.

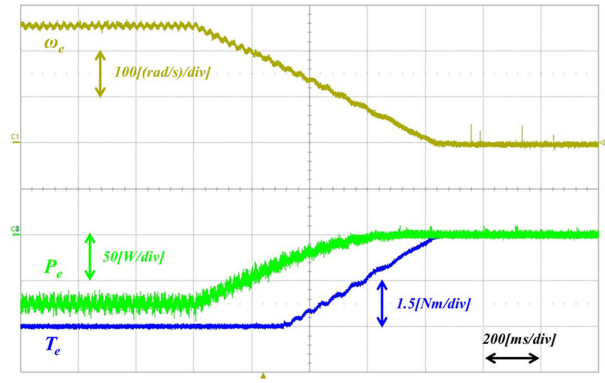

Fig. 32. Experimental results of the proposed MRPP-based braking for SPMSM.

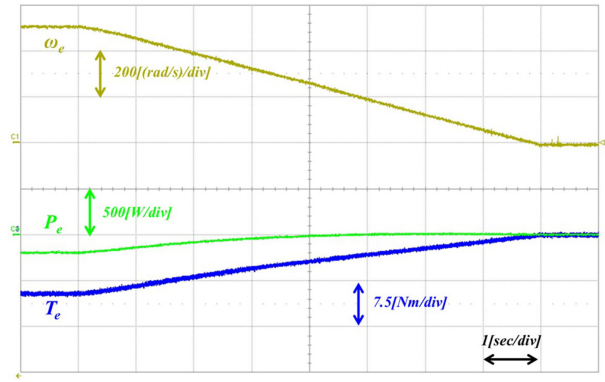

Fig. 33. Experimental results of the proposed MRPP-based braking for IPMSM.

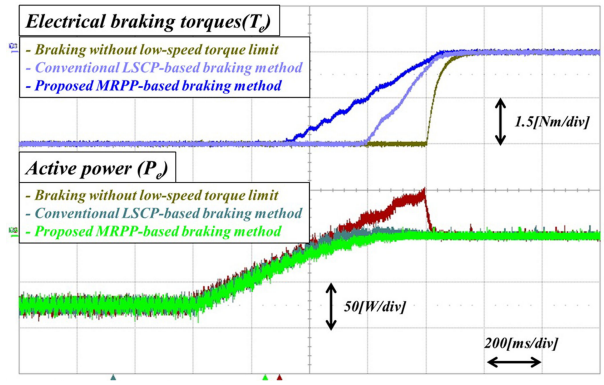

Fig. 34. Electrical braking torque and active power comparison of braking methods for SPMSM based on experimental results.

Using the memory function of the oscilloscope, the electrical braking torque and active power of the three aforementioned braking methods are compared for SPMSM and IPMSM as shown in Figs. 34 and 35. Since the memory is limited and the speed of the motor is almost the same no matter what braking method is used because of the speed-controlling load, the speeds are eliminated in this comparison. In this case, the experimental results are similar to the comparison in the simulation shown in Figs. 24 and 25. The proposed method achieves the highest regenerative power with the smallest braking torque, while the difference in active power is more significant for IPMSM

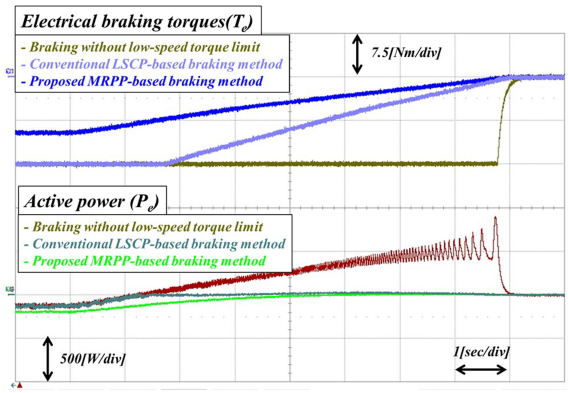

Fig. 35. Electrical braking torque and active power comparison of braking methods for IPMSM based on experimental results.

than SPMSM due to the difference in rated torque. However, unlike the simulation, the torque values and powers for IPMSM between the proposed method and the two other conventional methods are different to begin with because the initial speed of the motor is below the limit speed, and, for the proposed method, the torque follows the MRPP curve maximizing the regenerative power as mentioned earlier.

VI. Conclusion

In this article, a regenerative braking method based on the low-speed torque limit trajectory according to the MRPP curve is proposed. The proposed braking method is analyzed based on models of common motors along with a conventional LSCP-based method for comparison. As shown by simulation and experimental results, the proposed method regenerates more power with less electrical braking torque resulting in harvesting the maximum available regenerative power for the battery. Also, since this proposed braking method is only based on models for PMSMs, it can be implemented not only in electric vehicles but also in lots of other industrial applications such as flywheels or wind energy conversion systems. However, the proposed method is vulnerable to parameter variation of the motor because the proposed method is based on these parameters. Although the conventional table-based method was introduced in Section III to overcome inaccuracies caused by parameter variation, making a multi-dimensional table not only requires additional sensors and testing devices but also is a very time-consuming process. Therefore, further consideration and studies are required to compensate for the inaccuracy from the parameter variation more effectively.

References

[1] P. Fajri, S. Lee, V. A. K. Prabhala, and M. Ferdowsi, "Modeling and integration of electric vehicle regenerative and friction braking for motor/dynamometer test bench emulation," *IEEE Trans. Veh. Technol.*, vol. 65, no. 6, pp. 4264–4273, Jun. 2016.

[2] H. Yeo, D. Kim, S. Hwang, and H. Kim, "Regenerative braking algorithm for a HEV with CVT ratio control during deceleration," in *Proc. SAE CVT Congr.*, 2004, pp. 1–7.

[3] X. Zhang, D. Göhlich, and J. Li, "Energy-efficient toque allocation design of traction and regenerative braking for distributed drive electric vehicles," *IEEE Trans. Veh. Technol.*, vol. 67, no. 1, pp. 285–295, Jan. 2018.

[4] Y. Gao, L. Chu, and M. Ehsani, "Design and control principles of hybrid braking system for EV, HEV and FCV," in *Proc. IEEE Veh. Power Propulsion Conf.*, 2007, pp. 384–391.

[5] P. Fajri, S. Heydari, and N. Lotfi, "Optimum low speed control of regenerative braking for electric vehicles," in *Proc. IEEE 6th Int. Conf. Renewable Energy Res. Appl.*, 2017, pp. 875–879.

[6] S. Heydari, P. Fajri, I. Husain, and J. Shin, "Regenerative braking performance of different electric vehicle configurations considering dynamic low speed cutoff point," in *Proc. IEEE Energy Convers. Congr. Expo.*, 2018, pp. 4805–4809.

[7] P. Fajri, S. Heydari, and N. Lotfi, "Optimum low speed control of regenerative braking for electric vehicles," in *Proc. IEEE 6th Int. Conf. Renewable Energy Res. Appl.*, 2017, pp. 875–879.

[8] S. Heydari, P. Fajri, I. Husain, and J. Shin, "Regenerative braking performance of different electric vehicle configurations considering dynamic low speed cutoff point," in *Proc. IEEE Energy Convers. Congr. Expo.*, 2018, pp. 4805–4809.

[9] S. Heydari, P. Fajri, R. Sabzehgar, and M. Rasouli, "A novel approach for maximizing regenerative braking energy extraction of electric vehicles using motor performance lookup table," in *Proc. IEEE Transp. Electrific. Conf. Expo.*, 2019, pp. 1–5.

[10] S. Heydari, P. Fajri, M. Rasheduzzaman, and R. Sabzehgar, "Maximizing regenerative braking energy recovery of electric vehicles through dynamic low-speed cutoff point detection," *IEEE Trans. Transp. Electrific.*, vol. 5, no. 1, pp. 262–270, Mar. 2019.

[11] P. Suntharalingam, "Kinetic energy recovery and power management for hybrid electric vehicles," Ph.D. dissertation, Dept. Eng. Appl. Sci., , Cranfield Univ., Bedford, U.K., 2011.

[12] S. Heydari, P. Fajri, N. Lotfi, and B. Falahati, "Influencing factors in low speed regenerative braking performance of electric vehicles," in *Proc. IEEE Transp. Electrific. Conf. Expo.*, 2018, pp. 494–499.

[13] W. Kim, K. Choo, I. Won, J Kim, J. Lee, and C. Won, "A study on the regenerative braking method of permanent magnet synchronous motor for maximum regenerative power," in *Proc. 24th Int. Conf. Elect. Eng.*, Korea, 2018, pp. 929–934.

[14] K. Choo, W. Jeong, B. Kim, J. Park, J. Lee, and C. Won, "Maximum regenerative power braking for interior permanent magnet synchronous motor," in *Proc. IEEE Transp. Electrific. Conf. Expo., Asia-Pacific (ITEC Asia-Pacific)*, 2019, pp. 1–5.

[15] Y. Gao, L. Chen, and M. Ehsani, "Investigation of the effectiveness of regenerative braking for EV and HEV," *SAE Trans. J. Passenger Cars*, vol. 108, no. 6, pp. 3184–3190, 1999.

[16] K. H. Nam, *AC Motor Control and Electrical Vehicle Applications*, 2nd ed. Boca Raton, FL, USA: CRC Press, 2018.

Kyoung-Min Choo received the B.S. degree in automation system from Dongyang Mirae University, Seoul, Korea, in 2014. He is currently working toward the Ph.D. degree in electrical and computer engineering with Sungkyunkwan University, Suwon, Korea.

His research interests include control of synchronous machine drives and power conversion systems.

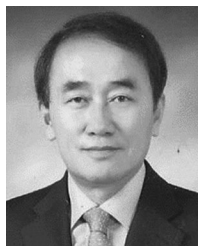

Chung-Yuen Won (Senior Member, IEEE) was born in Korea, in 1955. He received the B.S. degree from Sungkyunkwan University, Suwon, Korea, in 1978, and the M.S. and Ph.D. degrees from Seoul National University, Seoul, Korea, in 1980 and 1987, respectively, all in electrical engineering.

From 1990 to 1991, he was with the Department of Electrical Engineering, University of Tennessee, Knoxville, TN, USA, as a Visiting Professor. Since 1988, he has been a member of the Faculty of Sungkyunkwan University, where he is currently a Professor with the College of Information and Communication Engineering. Also, from 2008 to 2013, he was the Director with Samsung Energy Power Research Center. In 2010, he was the President with the Korean Institute of Power Electronics. Since 2016, he has been the Director with the DC Distribution Research Center. His current research interests include the power electronic of electric machines, electric/hybrid vehicle drives, and power converters for dc distribution systems.